Surface plasmons propagation along metallic rough diffraction gratings

Hugo Bruhier, Isabelle Verrier, Thiaka Gueye, Christelle Varenne, Amadou Ndiaye, Olivier Parriaux, Colette Veillas, Stéphanie Reynaud, Jérôme Brunet, Yves Jourlin

Surface plasmons propagation along metallic rough diffraction gratings

Hugo Bruhier[a], Isabelle Verrier[a], Thiaka Gueye[b], Christelle Varenne[b], Amadou Ndiaye[b], Olivier Parriaux[a], Colette Veillas[a], Stéphanie Reynaud[a], Jérôme Brunet[b], and Yves Jourlin[a]

[a]Université de Lyon, UJM, CNRS, IOGS, Laboratoire Hubert Curien, UMR CNRS 5516, 42000 Saint-Etienne, France
[b]Université Clermont Auvergne, CNRS, Sigma Clermont, Institut Pascal, F-63000 Clermont-Ferrand, France

ABSTRACT

In this work, the effect of roughness on surface plasmon propagation along metallic gratings is investigated. In the case of a shallow sinusoidal grating, modeling that takes into account the surface roughness shows the modification of the coupling properties of the plasmon modes. In the case of a deep sinusoidal rough grating, modeling of the SPR response is compared to the experimental one, showing a strengthening of the intra-coupling between forward and backward plasmon modes. This study demonstrates that the effect of the surface roughness on plasmon propagation must be considered especially in the case of deep gratings.

Keywords: Diffraction grating, plasmonics, roughness

1. INTRODUCTION

The surface plasmon resonance (SPR) effect is exploited since many years[1] for example as biological and environmental sensors.[2] SPR sensors present relevant characteristics particularly a good sensitivity to any changes in the refractive index of surrounding medium and are very competitive candidates to detect molecules, particles or to measure parameters such temperature or pressure. But, the sensitivity of the sensor could be affected by metal surface deffects like roughness. In this work, the effect of roughness on surface plasmons propagation along metallic gratings is investigated. Others authors had already experimentally shown that standard surface plasmon resonance is slightly shifted in the case of metal surface roughness.[3] In the present study, random Gaussian noise mimicking roughness is introduced in the simulation based on Chandezon's method,[4] which decomposes the grating surface profile by Fourier expansion. First, to compute the response of the rough surface, complex Fourier coefficients retrieved from the experimental surface profile are inserted into the simulation software[5] as well as the noise. Second, in the case of a shallow sinusoidal grating, simulation that takes into account the surface roughness shows the modification of the coupling properties of the plasmon modes; this change can be neglected most of the time. However at normal incidence, the modeling points out that the roughness has an influence on plasmon intra-mode coupling. Third, in the case of a deep sinusoidal rough grating, simulation of the optical response is compared to the experimental one. The grating was fabricated on a glass substrate by photolithography of the resist and thermal evaporation of the metal. Surface roughness induces a strengthening of the intra-mode coupling between forward and backward propagative plasmon modes and changes significantly the optical response of the metallic grating. Finally the conclusion demonstrates that the effect of the surface roughness on plasmon propagation must be considered especially in the case of deep structures.

Further author information: (Send correspondence to I.V or Y.J)
I.V.: isabelle.verrier@univ-st-etienne.fr
Y.J.: yves.jourlin@univ-st-etienne.fr

2. GRATING MODELING METHOD

To model the grating roughness three particular steps were needed (see fig.1). First the creation of a rough surface thanks to a convolution with a Gaussian kernel, second the Fourier series decomposition of this surface roughness and last the computation of this Fourier coefficients defining the surface in the software MC Grating,[5] based on Chandezon's method.[4] The Chandezon method first was developed in 1980 for modeling diffraction structures. The basis of the method is the use of Maxwell equations in covariant form in a curvilinear space where the profile become a plane. The purpose of such manipulation is the simplification of the boundaries condition. For unique interface Li et. al[6] proposed a simpler mathematical background and implementation without any tensorial algebra. The first step constituting the modeling of the rough surface is detailed in fig.2. A numerical library created a set of 1000 points distributed in one period as a random Gaussian noise as depicted in figure 2(a) with the noise in the left part and its Gaussian distribution of the right. The gaussian kernel with a width of $5.10^{-3}\,\Lambda$ is represented in fig.2(b) and is convoluted by the noise leading to resulting noise in fig.2(c).

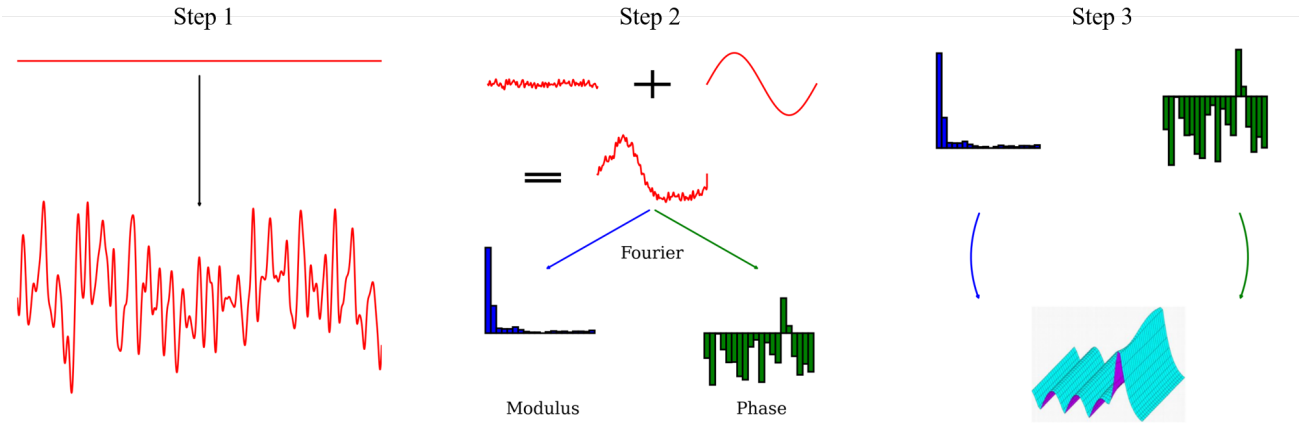

Figure 1. Scheme of the three different modeling steps for the computation of the theoretical response of rough gratings.

This noise is then added to a perfectly smooth sinusoidal profile to obtain those of the rough sinus grating (Step 2 of fig.1). The goal is then to find the Fourier coefficients c_n of this last profile that permit to fully define a 1-periodic profile function $p(x)$ as

$$p(x) = \sum_{i\in\mathbb{Z}} c_n \exp\left(j2\pi n x\right)\ ,\ c_n = \int_0^1 p(u)\exp\left(-j2\pi n u\right)\mathrm{d}u. \tag{1}$$

The computation of these complex coefficients is made numerically and then are separated into the modulus and the phase part allowing to insert them in the MC Grating software to define our profile (Step 3, fig.1). In the computation, the number of Fourier components (10) is taken to have enough terms to reach the convergence. The gratings which are modeled in the following are in gold of permittivity $\varepsilon_{\mathrm{Au}} = (-31.71 + 2.23\,j)$ at $\lambda = 850$ nm, which values are issued from MC Grating.

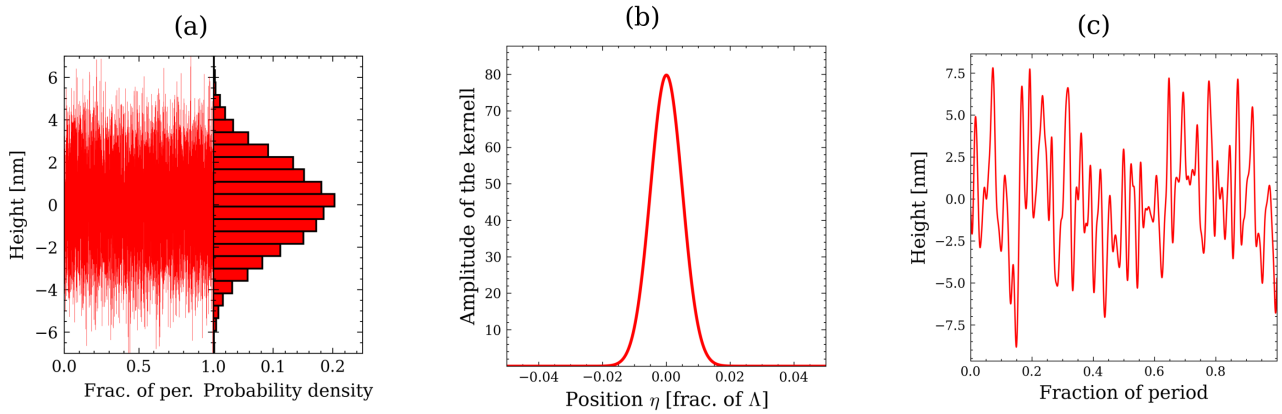

Figure 2. Gaussian correlated noise creation process (Step 1 of fig.1). (a) Uncorrelated numerically created gGussian noise and its computed distribution probability function. (b) Gaussian kernell used for convolution product with the initial noise. (c) Resulting noise of the convolution between the numerically created noise and the kernell.

3. MODELING OF SHALLOW GOLD GRATING

In this section we are interested in the modeling of shallow gold gratings in collinear and normal incidence and in the effect of a very high roughness on the plasmon resonance for such gratings. The quantity ζ, hereafter called the roughness ratio, quantifies how rough the grating surface is compared to its depth. ζ is equal to the R_a (arithmetical mean deviation of the rough surface $p^R(x)$ compared to the smooth surface $p^S(x)$ along the distance l) roughness parameter defined as

$$R_a = \frac{1}{l}\int_0^l \left|p^R(x) - p^S(x)\right| \mathrm{d}x\,, \tag{2}$$

which is divided by the peak-to-peak sinusoidal grating depth d: $\zeta = R_a/d$ and this ratio is introduced as a way to compare roughness grating profiles. First, we study a one dimensional shallow gold grating of period $\Lambda = 890$ nm and depth $d = 31$ nm illuminated under variable incidence $\theta \in [0;6]^\circ$ in air at a fixed wavelength $\lambda = 850$ nm under TM polarization as depicted in fig.3(a). The SPR coupling into the propagative plasmon mode occurs thanks to the $+1^{\text{st}}$ evanescent order of the grating and can be represented by the Ewald sphere (in red, fig.3(b)). The geometric construction of the Ewald sphere (in the spatial frequency reciprocal space) permits to link together the different optogeometrical parameters: the wavenumber k_0 of the incident TM beam, the grating vector $K_G = 2\pi/\Lambda$ and the propagation constant β of the plasmon mode (which propagates in a perpendicular direction compared to the grating lines at the metal-dielectric interface) according to the phase matching condition equation (3)

$$k_0\, n\, \sin(\theta) + m\, K_G = \pm\beta\,. \tag{3}$$

The roughness of the metallic surface will change the propagation constant β of the plasmon and hence modify the coupling conditions in terms of angle and/or wavelength. The reflected theoretical intensity of the 0^{th} order versus the incidence angle form 0° to 6° under TM polarization at $\lambda = 850$ nm is presented in figure 3(c) for both smooth and rough grating. The roughness parameter $R_a = 2.7$ nm of the rough grating corresponds to $\zeta = 9\%$ and comes from experimental data for lithography production process and is extremely high for such a grating depth. The smooth grating corresponds to a perfect sinusoidal profile with $R_a = 0$ nm, such profile is generally used in the grating computation software. The roughness of the grating surface induces a shift of the resonance angle from $\theta_S = 3.52^\circ$ to $\theta_R = 3.603^\circ$ ($\Delta\theta = 0.08^\circ$). The position of the resonances are found thanks to a polynomial fit of the curve in the very neighborhood of the resonance position. In such modeling results the uncertainty of such fitting is low enough to ignore it in the computation of the plasmon propagation constant. By assuming a quasi-lossless propagation, the plasmon mode effective index n_p is computed by

$$n_p = \frac{\beta}{k_0}\,, \tag{4}$$

using eq.(3) to calculate β by the coupling of the light with the $+1^{st}$ diffraction order. The corresponding effective indices for the smooth and the rough gratings are found to be respectively $n_S = 1.0164$ and $n_R = 1.0179$; these values point out the small change in the plasmon propagation speed.

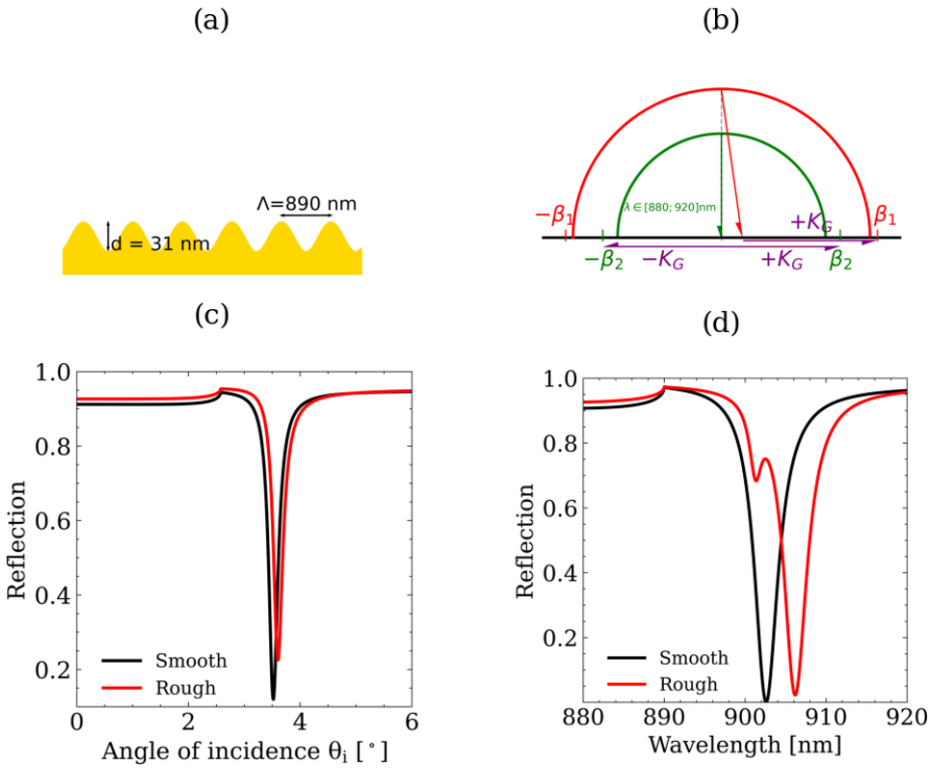

Figure 3. (a) Scheme grating with parameters $\Lambda = 850$ nm and $d = 31$ nm for the shallow gold grating. (b) Ewald sphere showing the coupling of the light in the surface plasmon via the evanescent $+1^{st}$ order or simultaneously with the $\pm1^{st}$ orders in normal indicence. (c) Angular modelled response of the 0^{th} order for the smooth (black curve, first from left) and for the rough (red, second from left) with R_a coefficient of 2.7 nm ($\zeta = 9\%$) in oblique TM incidence at $\lambda = 850$ nm. (d) Spectral responses in normal incidence for the same grating as (c).

A deeper understanding of the process needs the study of the spectral response of both smooth and rough gold gratings of the same parameters ($\Lambda = 850$ nm, $d = 31$ nm) in a wavelength range from 880 to 920 nm under TM fixed normal incidence. The reciprocal representation of this case given in fig.3(b) shows that, for an optimized sub-wavelength grating, there exist a possibility to excite simultaneously by the $\pm1^{st}$ diffractive orders the two propagative plasmon modes. The reflected intensity of the 0^{th} order is also presented in fig.3(d) for a smooth a rough grating, with the same roughness parameter R_a (and so ζ) as in fig.3(c). The rough grating case presents a curve split in plasmon resonance into two different dips, separated by a spectral distance $\Delta\lambda = 4.8$ nm, which corresponds to two different propagation constants, or effective indices of the two propagative modes $n_{R_1} = 1.0181$ and $n_{R_2} = 1.0127$. Hence, at normal TM incidence for a right choice of grating parameters, the two degenerate plasmons modes propagate in two opposite directions at two distinct speeds in the case of the rough grating.
The fig.4, which represents in false color the intensity values of the 0^{th} reflected order and the squared modulus of the electric fields at resonances illustrates this fact. Actually, under normal incidence for the rough gold grating, two distinct wavelengths $\lambda_{1R} = 901.35$ nm and $\lambda_{2R} = 906.15$ nm lead to plasmon resonance (fig.4(b)-(c)) unlike for the smooth grating, which exhibits a unique resonance (fig.4(a)) centered at $\lambda_{1S} = 902.6$ nm ($n_S = 1.0141$) between λ_{1R} and λ_{2R}. The squared electric fields are also represented in the smooth and rough case showing

a localisation of the field at the rough points of the profile for the rough grating whereas the field is located regularly on the smooth surface (fig.4(d)).

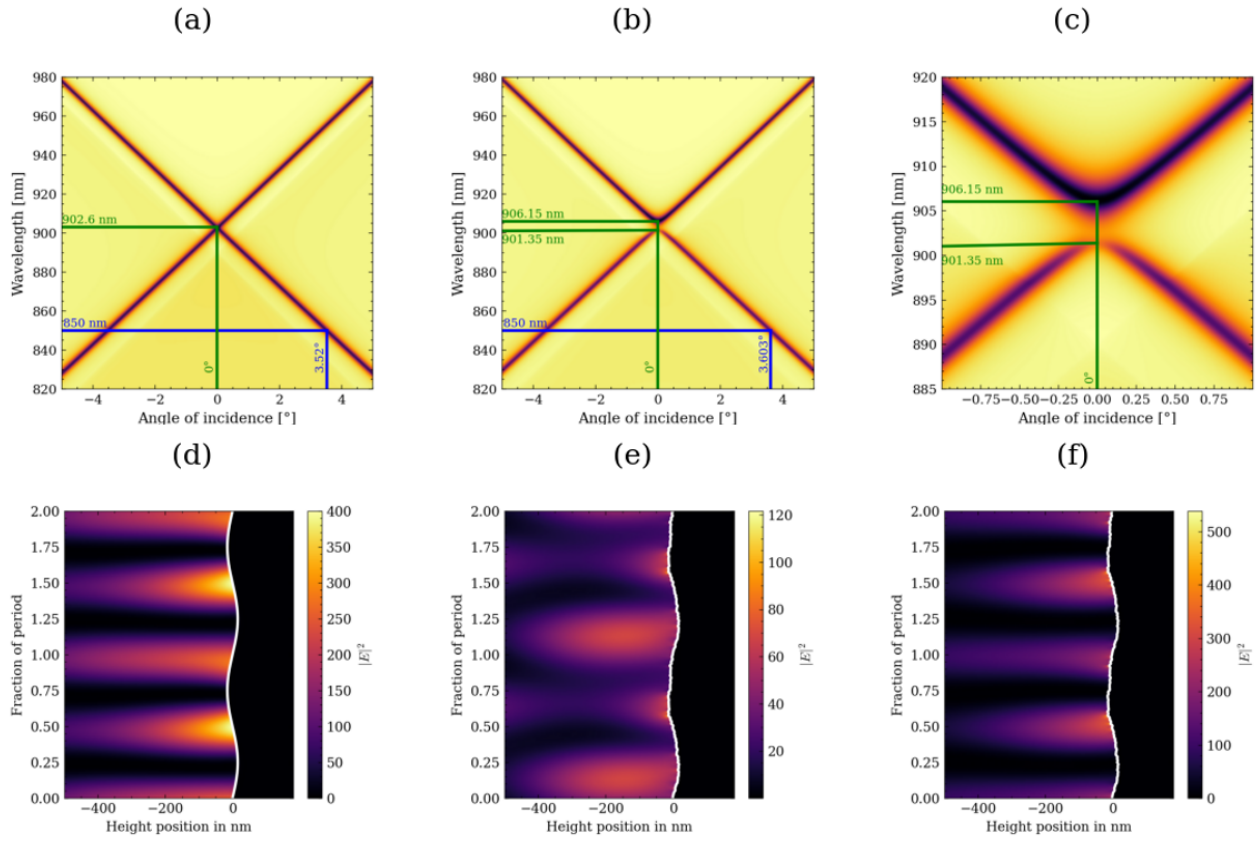

Figure 4. Plot of the reflected 0^{th} order in TM polarization in the neighborhood of the normal incidence versus incidence angle and wavelength for a shallow gold sinusoidal grating ($\Lambda = 850$ nm, $d = 31$ nm) in the (a) smooth and (b) rough ($R_a = 2.7$ nm) cases showing the resonance points presented in fig.3(c)-(d). (c) Zoom in the neighborhood of the center for the rough grating. (d) Squared modulus of the electric field for the smooth case at the (0°, 902.6 nm) point. (e)-(f) Squared modulus of the electric field in the rough case at the points (0°, 901.35 nm) (e) and (0°, 906.15 nm) (f).

4. MODELING AND MEASUREMENTS OF DEEP GOLD GRATING

The purpose of this part is to focus on the optical switching phenomenon, that only occurs with deep metallic gratings.[7] The basis of this effect is a transfer of energy between two reflected propagative orders, the 0^{th} and the -1^{st} orders. It is based, for deep gratings, on the multi-coupling of incident light into the propagative plasmon modes through the evanescent diffracted orders.[8] Historically, the shape of the -1^{st} was presented theoretically in a work where the plasmonic effect was not studied.[9] It was shown, thanks to a coupled mode formalism, that this so-called switching effect occurs because of interactions between forward and backward-propagative plasmon modes, such interactions being impossible with shallow gratings.

We showed in section 3 that, in case of a shallow metallic grating, the roughness of the surface modifies the propagation of the plasmon mode, visible through the modification of the resonance position (angle or wavelength). A change in the switching effect in the case of a deep rough grating is also expected and demonstrated in the following. In the example of fig.5(a) for a 1D sinusoidal gold deep grating ($\Lambda = 890$ nm, $d = 215$ nm) in TM incidence, the rough grating is studied angularly at $\lambda = 850$ nm. The modeled angular responses for the 0^{th} and -1^{st} diffracted orders are presented in fig.5(b) (grey and pink solid lines) for the rough (dashed lines)

for a grating of roughness parameter $R_a = 3$ nm. This roughness is very low in comparison to the depth and it corresponds to a ratio $\zeta = 1.4\%$. The minimum at $\theta^r_{+1} = 5.4°$ (rough) of the -1st order corresponds to the coupling through the +1st evanescent order to the forward-propagative plasmon and can be compared to the resonance angle $\theta_{+1} = 4.4°$ for the smooth grating, as depicted in fig.5(c). The other minimum of this order, at $\theta^r_{-2} = 59.4°$, corresponds to an excitation of the backward-propagative mode by the -2nd order (for the smooth grating $\theta_{-2} = 61.5°$), as shown in fig.5(d).

The resonance angles and computed effective indices for the smooth and rough gratings, retrieved with equation (3) show a marked change, even so the roughness ratio is very low ($\zeta = 1.4\%$), corresponding to a big shift in the resonance positions $\Delta\theta_{+1} = 1°$ ($\Delta n_{+1} = 0.0174$) and $\Delta\theta_{-2} = -2°$ ($\Delta n_{-2} = 0.0171$) when compared to the minor shift of $\Delta\theta = 0.08°$ ($\Delta n = 0.0015$) for the shallow grating of fig.3. Also, previously shown in section 3 for the shallow gold grating in normal incidence in fig.5(b)-(c), the inter-mode coupling in the rough case results in a gap existing beween the coupling conditions, and the rigorously computed plasmon resonance. The plasmon switching effect in deep metallic grating was shown to be created by inter-coupling[8] and the roughness can strengthen this coupling, permitting a greater modification of the resonance position than in shallow grating resonance, where such inter-mode coupling can only occurs at normal incidence.

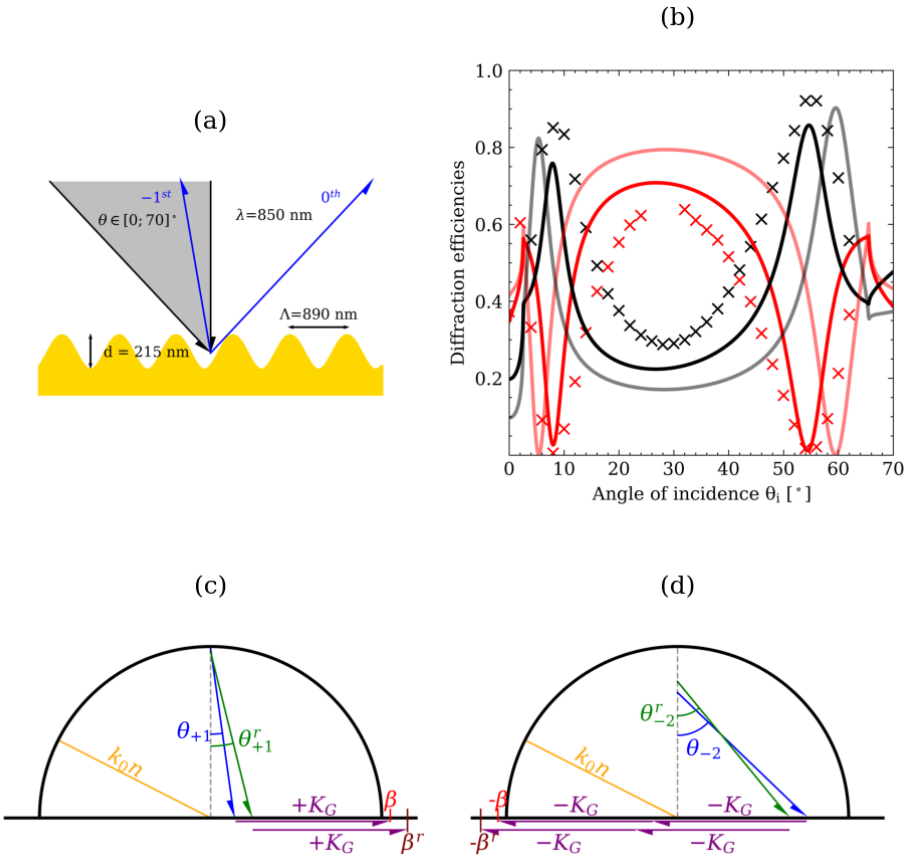

Figure 5. (a) Scheme of the incidence ($\theta \in [0; 70]°$, $\lambda = 850$ nm) and grating parameters ($\Lambda = 850$ nm, $d = 215$ nm) for the deep gold grating in TM polarization. (b) Experimental efficiencies (crosses) of the -1st (red crosses) ans the 0th (black crosses) reflected orders versus the incidence angle compared with simulations (in solid lines) for $\zeta = 1.4\%$ (grey curves) and $\zeta = 2.6\%$ (black curves) (c)-(d) The reciprocal Ewald sphere which represents coupling by the -2nd order to the backward-propagative plasmon mode and the coupling through the +1st forward-propagative in the smooth (at angles θ_{-2} and θ_{+1}) and rough (at angles θ^r_{-2} and θ^r_{+1}) cases.

The following idea is to confirm these simulations with experimental measurements. They were made using a photosensitive resist grating deposited on a glass subtrate. The resist was exposed to UV light and then revealed in a basic developer. Then the gold layer was deposited onto the grating through thermal evaporation technique in high vacuum (below 10^{-5} mbar) at a rate of 1 Å/s, controlled by a quartz crystal monitor. The thickness of the gold layer is approximately 120 nm, which permits to consider an infinite metallic layer and so avoid the influence of the photoresist layer. Also, the relatively low thickness of this layer induces a conformal coating. Atomic Force Microscopy (AFM) image in fig.6 permits to know the shape of the profile of the grating (fig.6(a)) and with the eq.(2) to estimate the experimental roughness coefficient as $R_a \approx 3 \pm 1$ nm ($\zeta = 1.4\%$) using the unstructured (plane) area of the same sample (fig.6(b)).

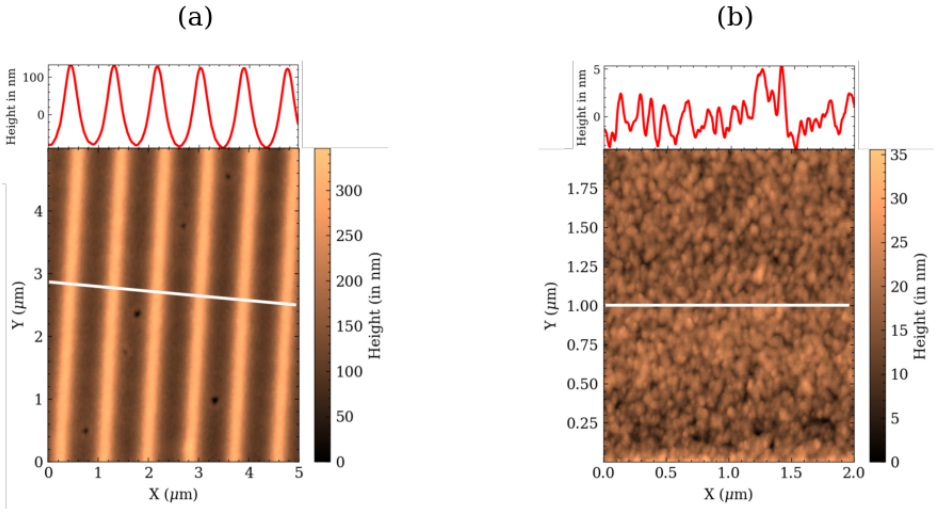

Figure 6. AFM images of (a): profile of the line for the deep gold grating ($\Lambda = 890$ nm, $d = 215$ nm); (b) profile of the flat gold coated surface.

The diffraction efficiencies measurement set-up was conceived so to achieve an angular TM interrogation of the diffraction grating, as shown in fig.7. The light issued from a laser diode (LD) at 850 nm is filtered by a hole H and illuminates the sample under TM polarization thanks to the polarizer P. The sample is oriented by a numerical goniometer and a rotating stage permits to set the IR photodiode in front of the reflected 0^{th} and -1^{st} orders. The output voltage delivered by the transimpedance circuit connected to the photodiode PD is measured by a NI9215 ADC module and analyzed by a computer. Measurement (crosses) of the two propagative diffraction orders are plotted in fig.5(b) versus the incidence angle and compared to the theoretical ones.

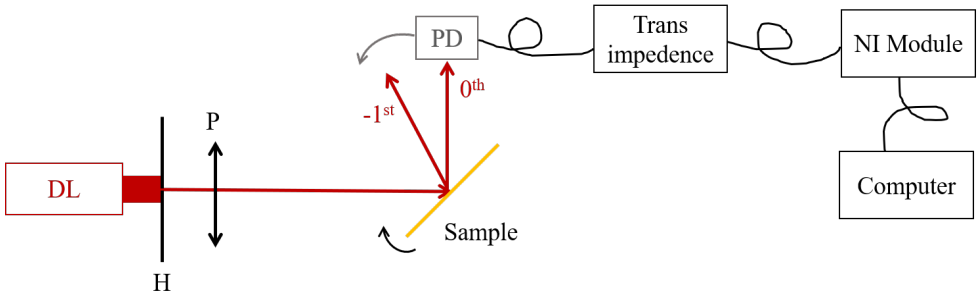

Figure 7. Set-up measurement; LD : Laser Diode, H : Hole, P : Polarizer, PD : Photodiode.

The modeled diffraction efficiencies for the roughness parameter determined by AFM (R_a = 3 nm, corresponding to a roughness ratio of $\zeta = 1.4\%$) (grey and pink curves) are not superimposed on the experimental one. So the roughness ratio was also adjusted to match experimental resonances positions ($\theta^e_{+1} = 8.2°$ and $\theta^e_{-2} = 54.8°$) which leads to a higher roughness ratio of $\zeta = 2.6\%$ (corresponding to R_a = 5.7 nm), this adjustment is made by a trials and errors approach (black and red curves in figure 5(b)). This corresponding value is higher than the one found in AFM but is also subject to some computation errors and uncertainties in the measurement of the resonances angles. These uncertainties in the angles of resonances σ_{theta_i} lead to an uncertainty in the calculated effective index σ_{n_p}, which is computed using propagation law of uncertainties[10] on the eq.(3) and is equal to

$$\sigma_{n_p} = \cos(\theta_i)\,\sigma_{\theta_i}. \tag{5}$$

The corresponding effective indices of the forward and backward propagative plasmon modes are then given by $n_{p_1} = 1.093 \pm 0.009$ and $n_{p_2} = 1.097 \pm 0.005$. Also the modeling method does not take into account all the imperfections of the grating, which is not perfectly uniform all around the probed area and which roughness could vary along several grating periods. Theses facts explain that, even if the curves of fig.5(b) shows the same tendency between experimental and theoretical diffraction efficiencies, the shapes differs in amplitude and have not the same resonances angles.

5. CONCLUSION

This work demonstrate the impact of roughness on the surface of a metal grating for SPR sensors. In the case of a shallow grating, the angular resonance shifts and broadenings for a fixed wavelength (angular scan) and splits into two spectral components at normal incidence (wavelength scan). Deeper gratings (more than a few hundred of nanometers) present angular resonances which get closer to each other as the roughness increases. By measuring the roughness of the sample and introducing the value in the model that we have developed, it is possible to calculate the resonance positions and to predict the behavior of the sensor.

ACKNOWLEDGMENTS

The authors want to thanks the financial support of this work by the French *Agence Nationale de la Recherche* (ANR) in the frameworkof the ANR CAPTAIN project (ANR-18-CE04-008). This work was also possible thanks to the means available within CNRS NanoSaintEtienne platform.

REFERENCES

[1] Maier, S. A., [*Plasmonics: fundamentals and applications*], Springer.
[2] Homola, J., "Surface plasmon resonance sensors for detection of chemical and biological species," **108**(2), 462–493.
[3] Shibata, T., Ikeda, H., Nishiyama, H., Tawa, K., and Nishii, J., "Optimization of metal quality for grating coupled surface plasmon resonance," **48**, 179–183.
[4] Chandezon, J., Raoult, G., and Maystre, D., "A new theoretical method for diffraction gratings and its numerical application," **11**(4), 235–241.
[5] Lyndin, N. and Usievich, B., "MC grating."
[6] Li, L., Chandezon, J., Granet, G., and Plumey, J.-P., "Rigorous and efficient grating-analysis method made easy for optical engineers," **38**(2), 304.
[7] Sauvage-Vincent, J., Jourlin, Y., Petiton, V., Tishchenko, A., Verrier, I., and Parriaux, O., "Low-loss plasmon-triggered switching between reflected free-space diffraction orders," **22**(11), 13314.
[8] Tishchenko, A. V. and Parriaux, O., "Coupled-mode analysis of the low-loss plasmon-triggered switching between the 0 th and -1 st orders of a metal grating," **7**(4), 1–9.
[9] Hutley, M. C., "An experimental study of the anomalies of sinusoidal diffraction gratings," **20**(8), 607–624.
[10] Ku, H., "Notes on the use of propagation of error formulas," **70C**(4), 263.